Minimal Curvature Variation Flow in Image Inpainting

by

Chun Ho Leung

A research paper
presented to the University of Waterloo
in partial fulfillment of the
requirement for the degree of
Master of Mathematics
in
Computational Mathematics

Supervisor: Prof. Justin Wan

Waterloo, Ontario, Canada, 2012

I hereby declare that I am the sole author of this report. This is a true copy of the report, including any required final revisions, as accepted by my examiners.

I understand that my report may be made electronically available to the public.

Abstract

Image inpainting is an important area in digital image processing, which has applications in problems like image restoration, scratch removal, or fluorescent microscopy. A lot of tools have been developed to tackle these problems. The total variation inpainting and the Euler's elastica model are popular variational PDE methods in nontexture local image inpainting. The former is developed from the model in which the inpainting solution minimizes the total variation in the intensity function, while the latter approximates the isophotes (curves of the same intensity value in an image) by elasticas, permitting the solution to have curved geometries.

These methods have been well-studied in two dimensions. It is natural to extend these methods to three dimensions, which is currently a popular research area in medical image processing.

This research paper aims to review the general ideas of the variational approach in image inpainting, and study the theory and properties of different models. The extension to three dimensional inpainting will also be discussed.

Based on the shortcomings of these models in different situations, we will introduce a new variational method, which tries to inpaint in such a way that the curvatures of isophotes are preserved. This new model behaves nicely in both two and three dimensions, and produces more desirable solutions in some cases, for example the cylinder inpainting problem in three dimensions, which we will describe along the way.

Acknowledgements

I would like to thank my advisor Prof. Justin Wan for his supervision in this project, and for his help throughout the year. I also want to thank Prof. Serge D'Alessio for his help in reading this report.

Dedication

This is dedicated to Ms. Poon Suet Fan.

Table of Contents

Chapter 1

Background

In this paper, we will study image inpainting, which is a type of problem frequently encountered in image processing. For example, suppose you have an image where there are some scratches, as in Figure 1.1.

Figure 1.1: Scratches in an image

It may not be hard for conservators or even ordinary people to "restore" the above image (namely, filling in what is missing in the scratches). The solution, however, is not entirely obvious if we want to do it digitally, due to the fact that no definitive solution is guaranteed. Even for two professional conservators, their restorations of the scratches will not be perfectly the same. Unlike finding the roots of a quadratic polynomial, there is no analytic solution to the inpainting problem. Very often, the solution is not unique.

Nevertheless, one can still formulate this as a mathematical problem. There are many methods in image inpainting (for example, the use of transport as in [1], splines as in [15],

or fast inpainting based on coherence transport as in [3]). Works on texture inpainting can be found in [8] and [9]. The general inpainting problem is described as follows.

Mathematically, let I be an image domain. A grey-level image can be fully characterized by a function

$$u : I \to [0, 1],$$

where 0 corresponds to "black" and 1 corresponds to "white". We do not usually assume that u is smooth. The intensity function u is sometimes assumed to be in the Sobolev space $H^1(I)$ or has bounded variation.

Suppose now a portion of I is removed. Namely, let $J \subset I$ be a subset of I. Our goal is to determine what $u|_J$ can be, given the information from $I \backslash J$. An example would be the following:

The small rectangular region filled with random signals is the region to be inpainted. To most human eyes, an obvious choice is to complete the disk. Namely, a pleasing solution will be:

One can of course argue that the original image can be anything. It is true that the inpainting problem is not well-posed, as illustrated in Figure 1.2. The region filled with random signal is the region to be inpainted.

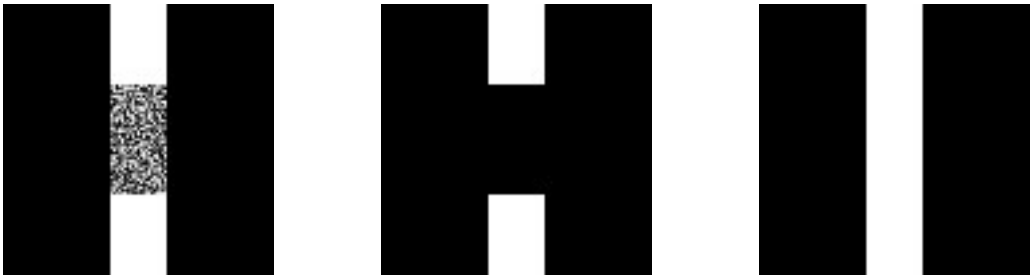

(a) Inpainting Problem (b) Solution A (c) Solution B

Figure 1.2: An inpainting problem

Even to the human eyes, both solutions A and B may make sense. There is no definitive answer to what the region should be. Unless we have a prior assumption of the image, it is unlikely that we can arrive at an answer. Each prior assumption corresponds to a model in image inpainting.

Chapter 2

Variational Methods

There are many existing methods in image inpainting. Textbook methods involve polynomial interpolation or harmonic. These models work well as long as the image is resonably smooth. But it is known that these methods are generally unable to recover edges well, because these are the "reasonable" discontinuities of the image. Also, practical images often contain noise and blurs, which will affect the performance of these inpainting models.

To tackle these difficulties, variational partial differential equation (PDE) methods have been suggested.

2.1 Total Variation (TV) Inpainting

Let I be an image domain and J be a missing region. Let $u^0 : I \to [0, 1]$ be the intensity function. The problem is to determine $u|_J$ from $u^0|_I$. Let u be a function. Following [6], and the related works [13] and [14] on image denoising, we define an energy

$$E(u) = \int_I |\nabla u| dx + \frac{\lambda}{2} \int_{I \setminus J} (u - u^0)^2 dx.$$

The first term corresponds to the total variation of u, whereas the second term is ($\frac{\lambda}{2}$ times) the squared L^2 distance of u and u^0.

The total variation inpainting method seeks to find $u \in BV(I)$ (i.e. all functions defined on I having bounded variations) such that $E(u)$ is minimized. Namely, we want to find

$$u = \text{argmin}_{v \in BV(I)} E(v).$$

To minimize the first term in the energy roughly means that we want u to be "as smooth as possible". In other words, we punish large variations in u. On the other hand, we also want to minimize the second term in the energy, which can be thought of as the distance between u and the original image. Including the consideration of the distance means we do not want to be too far away from the original image in the L^2 sense.

To solve for a minimizer of $E(u)$, one approach is to derive the Euler-Lagrange equation of this functional, and solve the equation for a local minimum.

Theorem 2.1.1. *Assume $\frac{\partial u}{\partial \nu} = 0$ on the boundary of I. The first variation of the functional $E(u)$ is given by*

$$V = -\nabla \cdot \frac{\nabla u}{|\nabla u|} + \lambda(x)(u - u^0),$$

where $\lambda(x) = \lambda$ if $x \in I \backslash J$ and 0 otherwise.

Proof. With $\lambda(x)$ defined above, we can write the TV functional as

$$E(u) = \int_I (|\nabla u| + \frac{\lambda(x)}{2}(u - u^0)^2)dx.$$

For a functional $\Omega(g)$, denote $\delta\Omega(g) = \frac{d}{d\epsilon}\Omega(g + \epsilon(\delta g))|_{\epsilon=0}$, the first variation of Ω at g under a pertubation from g to $g + \delta g$. For two vectors v and w, denote $\langle v, w \rangle$ to be their inner product. Now

$$\begin{aligned}
\delta E(u) &= \int_I (\delta[|\nabla u|] + \frac{\lambda(x)}{2}\delta[(u - u^0)^2])dx \\
&= \int_I (\frac{\langle \nabla u, \delta \nabla u \rangle}{|\nabla u|} + \lambda(x)(u - u^0)\delta u)dx \\
&= \int_I (\left\langle \frac{\nabla u}{|\nabla u|}, \nabla \delta u \right\rangle + \lambda(x)(u - u^0)\delta u)dx \\
&= \int_I (-\frac{\nabla \cdot \nabla u}{|\nabla u|}\delta u + \lambda(x)(u - u^0)\delta u)dx. \\
&= \int_I V \delta u dx
\end{aligned}$$

Note that in the second last equality we have integrated by parts and used the assumption that $\frac{\partial u}{\partial \nu} = 0$. □

Therefore, by the first optimality condition, to find local minima of the total variation functional, we have to solve the equation

$$-\nabla \cdot \frac{\nabla u}{|\nabla u|} + \lambda(x)(u - u^0) = 0.$$

This is a non-linear partial differential equation and is generally hard to solve. One can construct and solve a linear system using a fixed point method with $|\nabla u|$ delayed by one iteration. Alternatively, starting from an initial guess u, one can use the steepest descent method to evolve according to the equation

$$\frac{\partial u}{\partial t} = \nabla \cdot \frac{\nabla u}{|\nabla u|} + \lambda(x)(u^0 - u).$$

This is equivalent to evolving u in the direction of the steepest descent of the functional $E(u)$, until it stops at a stationary point. This does not, however, guarantee that we reach a global minimum, although in practice the steepest descent method works fine.

Recall the problem in Figure 1.2. The inpainting region is a rectangle with vertical length L and horizontal length l. Since $L > l$, in the noise-free TV model ($\lambda = \infty$), solution A is preferred to solution B.

As another example, consider the disk problem in Chapter 1. A portion of the disk is covered. If we use the TV inpainting model, we will get only a triangle joining the three extreme points on the boundary, instead of a circular disk(see Figure 2.1). This is expected, because all the variations can possibly come from the "edge" between the black and white regions, and hence the total variation is proportional to the length of the curve joining these two regions. Among all such curves, the one with shortest length is a straight line. Hence, the TV model will give us a straight line instead of an arc joining these two points.

2.2 TV Inpainting in 3D

In three dimensions, one can formulate an equivalent inpainting problem: Given a 3D region I where the intensity u on $J \subset I$ is missing, we have to determine what the intensity $u|_J$ can be using information from $u|_{I \setminus J}$, under some prior assumptions. For simplicity, we assume for now that the given information is noise free. If we would like $u|_J$ to have as

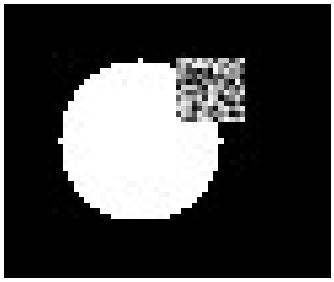

(a) Inpainting Problem

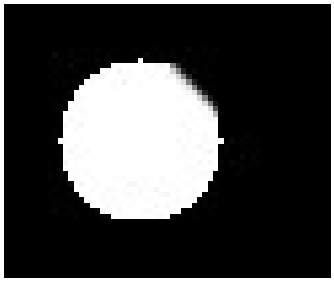

(b) TV Solution

Figure 2.1: The disk problem

little variation as possible, then the resulting model is a 3D version of the TV model, which minimizes

$$E(u) = \int_{J \cup \partial J} |\nabla u| dx.$$

The steepest descent is the same as that in the previous section. Namely, we evolve u from an initial guess u^0 under the Dirichlet problem

$$u_t = \nabla \cdot \frac{\nabla u}{|\nabla u|}, \quad u|_{\partial J} = u^0_{\partial J}.$$

Consider now a model problem of cylinder inpainting. Suppose we are given two ends of a cylinder and the middle part missing. What would happen if we run total variation inpainting in the region (see Figure 2.2)?

Clearly for any solution u, $|\nabla u(x)| = 0$ for all points $x \in I$ except those on the boundary of the solution. The discretized variation would then be equal to the intensity difference happening on the boundary of the solution. According to our scaling, the grey scale of a "white" region is 1 and that of a "black" region is 0. Therefore, the total variation of a solution u is the area of the boundary surface (in this case, the total variation functional is the same as the area functional of the boundary surface).

Therefore, the TV inpainting model amounts to finding the solution u with the minimum surface area in the middle region, such that the boundary agrees with the cylinder. This is exactly the classical minimal surface problem in geometry: finding critical points of the area functional.

Since the cylinder is rotationally symmetric around the z-axis, the minimal surface is also symmetric. It is well-known that (see for example [2] p.206) the only rotationally symmetric minimal surface in R^3 is the catenoid, which is defined by the parametric

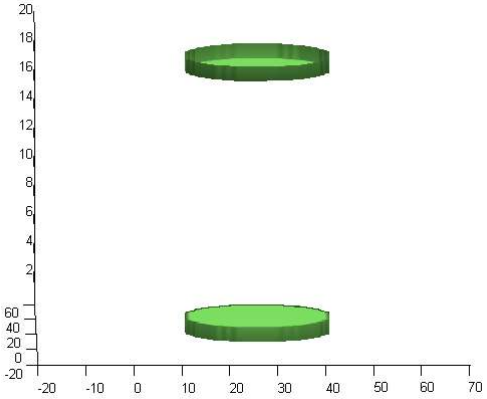

Figure 2.2: A cylinder with the middle part missing

equation

$$\begin{aligned} x &= c\cosh\frac{v}{c}\cos u \\ y &= c\cosh\frac{v}{c}\sin u \\ z &= v. \end{aligned}$$

Figure 2.3 is a cross section of a 3D image of a catenoid ($c = 0.7$).

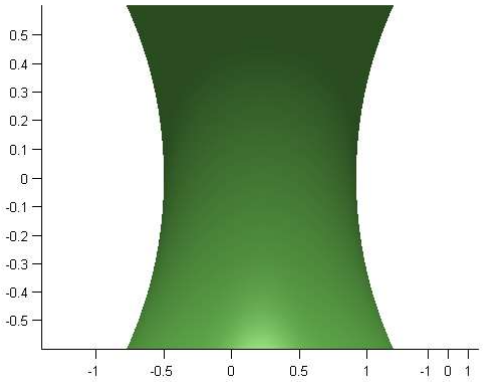

Figure 2.3: A catenoid

As seen from the figure, such a surface must inevitably be curved inwards. This means

that if we wanted to recover a cylinder given cylindrical boundary conditions, total variation inpainting will not be the right choice. We formulate this in the following

Theorem 2.2.1. *Suppose the height of the missing region is small enough such that TV inpainting gives a non-trivial solution. Then the solution of the TV inpainting model is given by a catenoid.*

Remark 2.2.2. The assumption that the height is small enough is necessary, because total variation inpainting suffers from the "relative size" property. If the missing region is too large, then TV would give a zero solution instead, because this would minimize the total variation (cf. the problem in Figure 1.2). Note that this solution is not smooth.

Figure 2.4 shows the TV filling of the middle part of the cylinder (we did solid TV inpainting, although here only the boundary is shown). The shape resembles that of a catenoid, as expected (i.e. curving inwards).

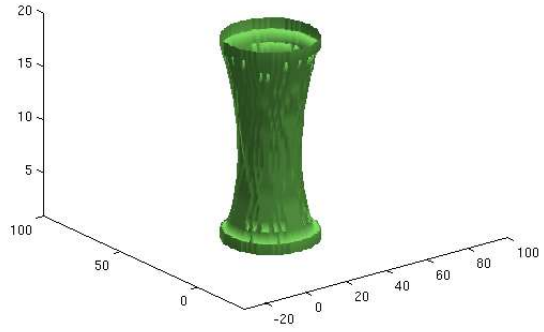

Figure 2.4: Total variation inpainting solution to the cylinder problem

2.3 Curvature in image processing

As seen in the previous section, despite its intuitive nature, the total variation model is unable to recover curved geometries. In order to do so, one has to develop a more sophisticated method. This section is intended for the understanding of curvature in images.

Let $u : I \subset \mathbb{R}^2 \to \mathbb{R}$ be a function. Assume for now that ∇u is non-zero everywhere. Then for any attainable c, by the implicit function theorem $u^{-1}(c)$ defines a regular curve.

If $x(t)$ is a parametrization of the curve, then from $u(x(t)) = c$ we have $\langle \nabla u, x'(t) \rangle = 0$. So ∇u defines a normal direction. The following theorem is an elementary result in differential geometry, and we include it here for completeness.

Proposition 2.3.1. *The curvature of the level curve $u^{-1}(c)$ with respect to the normal direction ∇u is given by*

$$\kappa = \nabla \cdot \frac{\nabla u}{|\nabla u|}.$$

In an image, at a given point, κ is the curvature of the curve through that point having the same grey value (isophote). An isophote can be an edge or an object, which are often characterised by their grey values. Thus κ is an indicator of how curvy the isophotes of an image are. For example, straight lines have zero curvature, while a circle of radius r have constant positive curvature $\frac{1}{r}$.

When $\kappa > 0$, the curve bends "away" from the normal direction $|\nabla u|$. An example is the circle, which always curves away from the outer normal. When $\kappa = 0$, the curve is intuitively a momentary straight line. When $\kappa < 0$, the isophote curves towards the normal direction. Humans eyes are able to detect the sign of the curvature.

In practice, ∇u may be zero, in which case κ will be undefined. Therefore, we will consider the following approximation of the curvature:

$$\kappa_\epsilon = \nabla \cdot \frac{\nabla u}{|\nabla u| + \epsilon},$$

for some small number ϵ. It is clear that if κ is defined (i.e. $\nabla u \neq 0$), then

$$\kappa = \lim_{\epsilon \to 0} \kappa_\epsilon.$$

In the numerical experiments, we will use κ_ϵ as a substitute for κ.

In three dimensions, the notion of curvature is more complicated. Let S be a surface in $\mathbb{R}^3$. At any point $p \in S$, among all directions you can move on the surface, there is one direction with the maximum curvature, and one with the minimum. The sum of these two curvatures is called the mean curvature (up to a factor of 2, depending on the convention), while the product of these two curvatures is called the Gaussian curvature.

If S is defined by an equation $u(x, y, z) = c$, then the mean curvature is also given by

$$\kappa = \nabla \cdot \frac{\nabla u}{|\nabla u|},$$

which is the same formula as that of a curve in $\mathbb{R}^2$.

Thus, the mean curvature of a sphere in $\mathbb{R}^3$ of radius r is given by $\frac{2}{r}$, while that of a cylinder with base radius r is given by $\frac{1}{r}$.

Recall that the steepest descent scheme of the total variation inpainting is given by the equation

$$u_t = \nabla \cdot \frac{\nabla u}{|\nabla u|}.$$

The study by Marquina and Osher in [12] shows that a factor of $|\nabla u|$ helps accelerate the TV inpainting, and will achieve an equivalent equilibrium. Namely, the inpainting is done by

$$\begin{aligned} u_t &= |\nabla u| \nabla \cdot \frac{\nabla u}{|\nabla u|} \\ &= |\nabla u| \kappa \end{aligned}$$

This is exactly the mean curvature motion for level sets, which is well-studied in the contemporary Mathematical literature (one of the first significant papers on this is [10]). In other words, the total variation inpainting coincides with the mean curvature flow.

2.4 CDD Inpainting

As discussed before, using total variation inpainting, the solution to the inpainting problem in Figure 2.5 is solution A, because the horizontal size of the rectangle is less than its vertical size. TV inpainting depends highly on the relative gap size to the surrounding objects, so in cases like that in Figure 2.5, "broken" objects may not be connected.

To solve this "problem" in TV inpainting, consider solutions A and B in terms of isophotes (level sets). The isophotes in solution A are broken with 4 corners, while the isophotes in solution B are smooth. Since corners have large curvatures, one way to prevent large curvatures from happening is to connect the broken bar.

In the TV model, one evolves u with the equation

$$u_t = \nabla \cdot \frac{\nabla u}{|\nabla u|}.$$

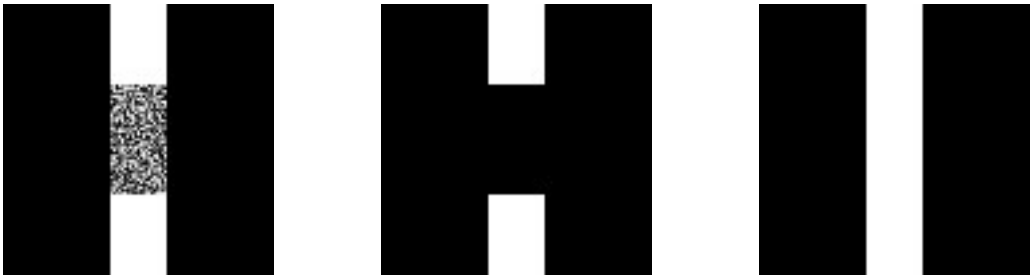

(a) Inpainting Problem (b) Solution A (c) Solution B

Figure 2.5: The inpainting problem in Figure 1.2

We can interpret this as a diffusion process, with diffusivity equal to $\frac{1}{|\nabla u|}$. Following [5], instead of $\frac{1}{|\nabla u|}$, we consider the new diffusion strength $\frac{|\kappa|^p}{|\nabla u|}$, for $p > 0$. Intuitively, the diffusion is stronger when the curvature of an isophote is large, and weaker when the curvature is small.

This gives us another inpainting scheme, known as the Curvature-Driven Diffusion (CDD) inpainting, which can connect broken objects even if the relative size requirement is not satisfied. The new scheme reads:

$$u_t = \nabla \cdot \frac{|\kappa|^p \nabla u}{|\nabla u|}, \quad p > 0.$$

Geometrically, then, TV inpainting and the CDD inpainting represent two different philosophies in inpainting. TV seeks to find the solution with smallest variation in intensity, while the CDD always seeks to connect broken objects. However, a problem still remains. Similar to TV inpainting, the CDD inpainting still tends to connect with straight lines (see [7] p.302). It is then desirable to have an inpainting model that can give us "curved" solutions when required. It turns out that the CDD can be incorporated into another model, which can produce "curvy" isophotes.

2.5 Euler's elastica inpainting

Instead of directly modifying the flow equation as is in CDD inpainting, another option is to modify the functional. Recall that the TV inpainting minimizes the functional

$$E_{TV}(u) = \int_I |\nabla u| dx + \frac{\lambda}{2} \int_{I \setminus J} (u - u^0)^2 dx.$$

The study in [4] considered a modification of the above energy to include the curvature. Let a, b be positive constants. Define the elastica energy to be

$$E(u) = \int_I (a + b\kappa^2)|\nabla u| dx + \frac{\lambda}{2} \int_{I \setminus J} (u - u^0)^2 dx,$$

where $\kappa = \nabla \cdot \frac{\nabla u}{|\nabla u|}$ is the (mean) curvature of level sets of u.

Equivalently, assuming the given part of the image is noise-free (i.e. we will not change that part), we can work with

$$E(u) = \int_I (a + b\kappa^2)|\nabla u| dx.$$

The a-part of the energy corresponds to that of the total variation, while the b-part of the energy corresponds to minimizing the curvature of the isophotes. Large curvatures will be punished, as in the CDD model.

Define $\lambda(x) = \lambda$ if $x \in I \setminus J$ and 0 otherwise. The steepest descent equation of the energy $E(u)$ is

$$u_t = \nabla \cdot V - \lambda(x)(u - u_0),$$

where

$$\begin{aligned} V &= (a + b\kappa^2)\mathbf{n} - P(\frac{1}{|\nabla u|} \nabla (2b\kappa |\nabla u|)), \\ \mathbf{n} &= \frac{\nabla u}{|\nabla u|}, \\ P(x) &= x - \langle x, \mathbf{n} \rangle \mathbf{n}. \end{aligned}$$

With this functional, the inpainting model tries to extend isophotes into the inpainting domain by Euler's elasticas, which are known as stationary curves of the energy

$$E_1(\gamma) = \int_\gamma (a + b\kappa^2) ds,$$

where ds denotes the arc length element. Euler's elasticas are smooth and can have curvatures (controlled by the magnitude of b). In contrast, the stationary curves of

$$E_2(\gamma) = \int_\gamma ds = \text{length}(\gamma)$$

are clearly linear. This explains why TV inpainting, in general, favours connection by straight lines. The change from the TV energy to the elastica energy effectively cooresponds to the change of our prior model of curves. In the TV model the isophotes are modelled by straight lines while in the elastica inpainting the isophotes are modelled by Euler's elasticas. Thus, if "curvy" solutions are required the elastica inpainting would be a more appropriate choice.

The elastica inpainting depends highly on the ratio of b to a in the energy. If $b \gg a$, then smoother isophotes will be obtained (see Figure 2.6).

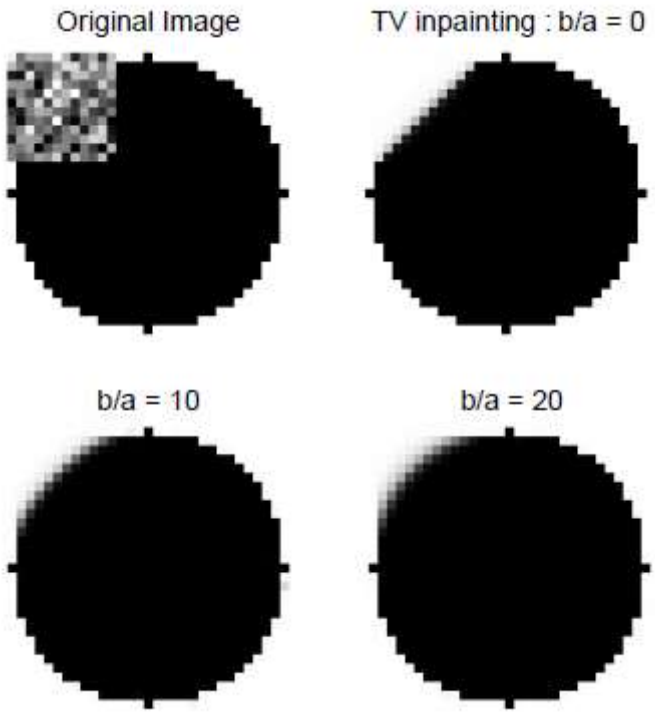

Figure 2.6: Effect of b/a on results in Euler's elastica inpainting

Note that when $b = 0$, the elastca model reduces to TV inpainting. Also, the CDD model is beautifully embedded in the Euler's elastica model in a natural way. In the Euler's elastica model, we consider the flux

$$V = (a + b\kappa^2)\mathbf{n} - P(\frac{1}{|\nabla u|}\nabla(2b\kappa|\nabla u|)).$$

We can write $V = V_{\mathbf{n}} + V_{\mathbf{t}}$, where

$$V_{\mathbf{n}} = (a + b\kappa^2)\mathbf{n},$$

$$V_{\mathbf{t}} = -P(\frac{1}{|\nabla u|}\nabla(2b\kappa|\nabla u|))$$

are respectively the normal part and tangential part of V. The normal divergence is equal to

$$\nabla \cdot V_{\mathbf{n}} = \nabla \cdot (\frac{a + b\kappa^2}{|\nabla u|}\nabla u)$$

since $\mathbf{n} = \frac{\nabla u}{|\nabla u|}$, which is similar to the flow equation in the CDD model:

$$u_t = \nabla \cdot \frac{|\kappa|^p \nabla u}{|\nabla u|}, p > 0.$$

Therefore, if $b \gg a$, properties of CDD (i.e. ability to connect) will become more apparent, as demonstrated in the Figure 2.7.

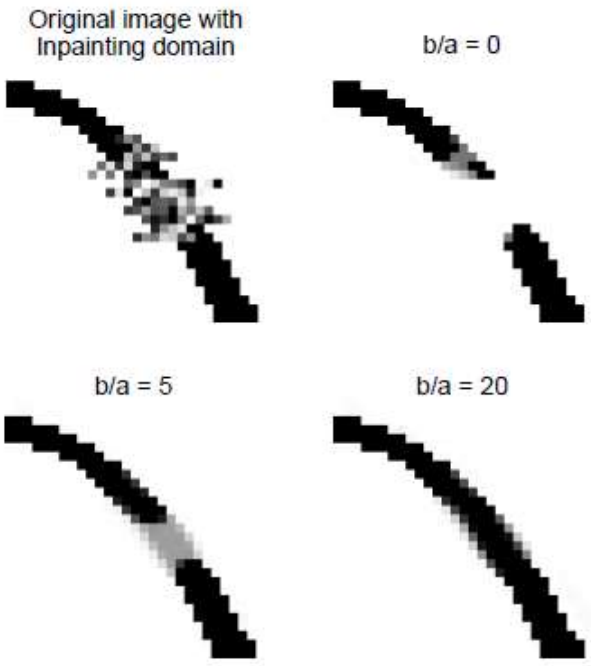

Figure 2.7: Effect of b/a on connectivity in Euler's elastica inpainting.

2.6 Euler's elastica inpainting in 3D

Now we return to the cylinder problem in Figure 2.2. An elementary result in classical differential geometry states that a minimal surface has zero mean curvature. In our context, this corresponds to $\kappa = 0$, analytically in the interior region.

A TV solution does not only (locally) minimize the variation. When analytic equilibrium is achieved, the steady state satisfies

$$\nabla \cdot \frac{\nabla u}{|\nabla u|} = 0,$$

i.e. $\kappa = 0$. Recall that the Euler's elastica model seeks to minimize

$$E(u) = \int_I (a + b\kappa^2)|\nabla u| dx.$$

When the first term is already a local minimum and the second term is mostly zero in the interior, there is no reason to believe that a cylinder can be recovered by the Euler's elastica method when generalized, that is, with the same formula of κ (see Figure 2.8).

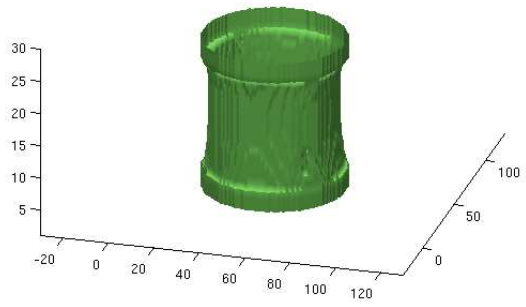

Figure 2.8: Euler's elastica solution of the cylinder problem

Chapter 3

Minimal Curvature Variation Flow (MCVF)

3.1 The functional

Inspired by [16], the motivation of the model is originally based on the lack of sensitivity of the total variation model to the digital curvature of the image. In order to have curved geometries, one has to take into account the curvature. The elastica inpainting is a good choice in this aspect.

As described before, the presence of the curvature in Euler's elastica functional seeks to punish large curvatures. Thus, smoother isophotes can be obtained. However, there is no apparent reason why we have to minimize the curvature whenever possible. It is true that this permits smoother isophotes, but the problem associated with this becomes apparent when we consider its direct generalization in three dimensions. A minimization of the (mean) curvature will distort the cylinder. One solution to this is to consider preserving the curvature, instead of minimizing it.

In this model, we want to minimize the change of curvature in the inpainting area along every level curve (or within any level area) of the intensity function.

Let I be the image domain, and $u : I \to [0, 1]$ be the intensity function. Then the digital curvature of u is defined by

$$\kappa = \nabla \cdot \frac{\nabla u}{|\nabla u|}.$$

For now, let us first assume that u is regular, i.e. ∇u is never 0. Then κ exists and is defined everywhere on I. By the implicit function theorem, the equation $u(x) = c$ defines a regular curve for every attainable c. On any such level curve, its curvature is given by κ.

Now we consider the functional

$$\Phi(u) = \int_0^1 \int_{u(x,y)=c} |\nabla\kappa|^2 ds dc,$$

where ds denotes the arc-length integral, and dc denotes the differential element across level sets, i.e. the cotangent dual to ∇u. This is the total change of curvature (square L^2 norm) on level sets.

On any level curve $u(x, y) = c$, by the assumption that $|\nabla u| \neq 0$ and the inverse function theorem, we have a unique anti-clockwise vector field e_1 satisfying $|e_1| = 1$. Depending on the convention, the normal vector can be written as $\pm\frac{\nabla u}{|\nabla u|}$. Denote $e_2 = \frac{\nabla u}{|\nabla u|}$.

Clearly e_1 and e_2 form an orthonormal basis at each point they are defined, so their duals e^1 and e^2 satisfy $e^1 \wedge e^2 = dx \wedge dy$, where $\wedge$ is the wedge product of differential forms.

Since $|e_1| = 1$, we have that $e^1 = ds$. Similarly $dc = |\nabla u| e^2$. Therefore, we can simplify the functional as follows:

$$\begin{aligned}
\Phi(u) &= \int_0^1 \int_{u(x,y)=c} |\nabla\kappa|^2 ds dc \\
&= \int_0^1 \int_{u=c} |\nabla\kappa|^2 |\nabla u| e^1 \wedge e^2 \\
&= \int\int |\nabla\kappa|^2 |\nabla u| dx dy
\end{aligned}$$

This is the energy we consider in this study. In other words, we seek inpainting solutions that minimize (at least locally)

$$\Phi(u) = \int\int |\nabla\kappa|^2 |\nabla u| dx dy.$$

This has the property that it punishes large variation of the digital curvature along level sets.

Suppose the inpainting domain contains a curved isophote, as in Figure 2.1. The curvature of a circle is $\frac{1}{R}$, where R is the radius. If we want to minimize the change of

curvature, a global minimum of the function will be given by the exact disk. We will show in section 3.4 that a disk can be well recovered by the MCVF.

The same idea applies to three dimensional inpainting. The cylinder has a constant mean curvature of $\frac{1}{R}$. The direct generalization of Euler's elastica will not preserve this, while the MCVF respects the mean curvature in this case. This claim will also be confirmed in section 3.6.

3.2 Derivation of the Euler-Lagrange equation

In this section we will work with the Euler-Lagrange equation of the aforementioned functional.
Let $J \subset I$ be the inpainting region.

Theorem 3.2.1. *Assume* $\nabla\kappa = \nabla(\nabla \cdot (|\nabla u|\nabla\kappa)) = 0$ *on the boundary of* J. *Then the first variation of the functional* Φ *is given by* $-\nabla \cdot V$, *where*

$$\begin{aligned} V &= \frac{2}{|\nabla u|} P(\nabla(\nabla \cdot (|\nabla u|\nabla\kappa))) + |\nabla\kappa|^2 \mathbf{n}, \\ P(x) &= x - \langle x, \mathbf{n}\rangle \mathbf{n}, \\ \mathbf{n} &= \frac{\nabla u}{|\nabla u|}. \end{aligned}$$

Proof. For a functional $\Psi(u)$ and a given u_0, denote

$$\delta\Psi(u_0) := \frac{\partial}{\partial t}\Psi(u_0 + t\delta u)|_{t=0},$$

which is the first variation at u_0 under the perturbation from u_0 to $u_0 + \delta u$.
We also denote by $\langle f \rangle = \int f$, following the notation in [4]. Now for the functional

$$\Phi(u) = \int\int |\nabla\kappa|^2 |\nabla u| dxdy,$$

we have

$$\begin{aligned} \delta\Phi(u) &= \left\langle \delta(|\nabla\kappa|^2|\nabla u|) \right\rangle \\ &= \left\langle \delta(|\nabla\kappa|^2)|\nabla u| \right\rangle + \left\langle |\nabla\kappa|^2 \delta|\nabla u| \right\rangle \\ &= \left\langle 2\left\langle \nabla\kappa, \delta\nabla\kappa \right\rangle |\nabla u| \right\rangle + \left\langle |\nabla\kappa|^2 \delta|\nabla u| \right\rangle \\ &= \left\langle 2\left\langle |\nabla u|\nabla\kappa, \nabla\delta\kappa \right\rangle \right\rangle + \left\langle |\nabla\kappa|^2 \delta|\nabla u| \right\rangle \\ &= -2\left\langle \nabla \cdot (|\nabla u|\nabla\kappa)\delta\kappa \right\rangle + \left\langle |\nabla\kappa|^2 \delta|\nabla u| \right\rangle, \end{aligned}$$

where the last line follows from the integration by parts, and the assumption that $\nabla\kappa = 0$ along the boundary.

Now we compute $\delta\kappa$:

$$\begin{aligned}
\delta\kappa &= \delta(\nabla \cdot \frac{\nabla u}{|\nabla u|}) \\
&= \nabla \cdot (\frac{1}{|\nabla u|}\delta(\nabla u) + \nabla u(\delta(\frac{1}{|\nabla u|}))) \\
&= \nabla \cdot (\frac{1}{|\nabla u|}\nabla(\delta u) - \frac{\langle \nabla u, \delta(\nabla u)\rangle}{|\nabla u|^3}\nabla u) \\
&= \nabla \cdot (\frac{1}{|\nabla u|}\nabla(\delta u) - \frac{\langle \nabla u, \nabla(\delta u)\rangle}{|\nabla u|^3}\nabla u) \\
&= \nabla \cdot (\frac{1}{|\nabla u|}P(\nabla(\delta u))) = \nabla \cdot (\frac{1}{|\nabla u|}P(\nabla(\delta u))),
\end{aligned}$$

where P is the projection onto the tangential component defined before, and if we write $\mathbf{n} = \frac{\nabla u}{|\nabla u|}$, it can be rewritten as

$$x = \frac{\langle x, \nabla u\rangle}{|\nabla u|^2}\nabla u + Px.$$

Thus the tangential part is

$$\delta\kappa = \nabla \cdot (\frac{1}{|\nabla u|}P(\nabla(\delta u))). \tag{3.1}$$

Next we have that

$$\delta|\nabla u| = \frac{\langle \nabla u, \nabla \delta u\rangle}{|\nabla u|} = \langle \mathbf{n}, \nabla \delta u\rangle, \tag{3.2}$$

where $\mathbf{n} = \frac{\nabla u}{|\nabla u|}$.

With (3.1), (3.2) and applying integration by parts successively, we get

$$\begin{aligned}
\delta\Phi(u) &= -2\left\langle \nabla\cdot(|\nabla u|\nabla\kappa)\delta\kappa\right\rangle + \left\langle |\nabla\kappa|^2\delta|\nabla u|\right\rangle \\
&= -2\left\langle \nabla\cdot(|\nabla u|\nabla\kappa)\nabla\cdot(\frac{1}{|\nabla u|}P(\nabla(\delta u)))\right\rangle + \left\langle |\nabla\kappa|^2\left\langle \mathbf{n},\nabla\delta u\right\rangle\right\rangle \\
&= 2\left\langle\left\langle \nabla(\nabla\cdot(|\nabla u|\nabla\kappa)),\frac{1}{|\nabla u|}P(\nabla(\delta u))\right\rangle\right\rangle - \left\langle\nabla\cdot(|\nabla\kappa|^2\mathbf{n})\delta u\right\rangle \\
&= 2\left\langle\left\langle \frac{1}{|\nabla u|}P(\nabla(\nabla\cdot(|\nabla u|\nabla\kappa))),\nabla(\delta u)\right\rangle\right\rangle - \left\langle\nabla\cdot(|\nabla\kappa|^2\mathbf{n})\delta u\right\rangle \\
&= -2\left\langle \nabla\cdot(\frac{1}{|\nabla u|}P(\nabla(\nabla\cdot(|\nabla u|\nabla\kappa))))\delta u\right\rangle - \left\langle\nabla\cdot(|\nabla\kappa|^2\mathbf{n})\delta u\right\rangle \\
&= \left\langle -(\nabla\cdot V)\delta u\right\rangle,
\end{aligned}$$

where we defined

$$V = \frac{2}{|\nabla u|}P(\nabla(\nabla\cdot(|\nabla u|\nabla\kappa))) + |\nabla\kappa|^2\mathbf{n}.$$

Notice that we have further used the assumptions that

$$\nabla(\nabla\cdot(|\nabla u|\nabla\kappa)) = \nabla\kappa = 0$$

on the boundary. □

Remark 3.2.2. For regularity, we will sometimes add a TV-regularizing term to the functional. The combined functional is

$$\Phi(u) = \int\int (a + b|\nabla\kappa|^2)|\nabla u|dxdy,$$

where $\frac{b}{a}$ is large. The resulting steepest descent equation is

$$\frac{\partial u}{\partial t} = a\kappa + b\nabla\cdot V,$$

where V is as described in Theorem 3.2.1.

3.3 Numerical Methods

In this section we present our discretization for $\nabla\cdot V$, where

$$V = \frac{2}{|\nabla u|}P(\nabla(\nabla\cdot(|\nabla u|\nabla\kappa))) + |\nabla\kappa|^2\mathbf{n}.$$

We compute the curvature in a way suggested in [14]. Let v be a function, and h, k be the spatial step sizes of the x and y directions, respectively. Denote $D_i^+ v$ to be the forward finite difference of v in coordinate i, and $D_j^- v$ to be the backward finite difference of v in coordinate j. Let

$$m_i = \text{minmod}(D_i^+ u, D_i^- u),$$

for $i = 1, 2$, where

$$\text{minmod}(a, b) = (\frac{\text{sgn}\, a + \text{sgn}\, b}{2}) \min(|a|, |b|).$$

The curvature $\kappa = \nabla \cdot \frac{\nabla u}{|\nabla u|}$ is computed using

$$\kappa_{i,j} \approx D_x^-(\frac{D_x^+ u}{D_x^+ u + m_2^2})_{i,j} + D_y^-(\frac{D_y^+ u}{D_y^+ u + m_1^2})_{i,j}.$$

Next we have to compute $\nabla \cdot (|\nabla u| \nabla \kappa)$. This is done using a half-point discretization. Denote $g = \nabla u$. We approximate

$$g_{i+\frac{1}{2},j} \approx \frac{g_{i+1,j} + g_{i,j}}{2}.$$

Similarly, $g_{i-\frac{1}{2},j}$ and $g_{i,j\pm\frac{1}{2}}$ are done by averaging. We also have to specify half-points for $\nabla \kappa$:

$$(\kappa_x)_{i+\frac{1}{2},j} = \frac{\kappa_{i+1,j} - \kappa_{i,j}}{h}$$

Similarly we can evaluate $(\kappa_x)_{i-\frac{1}{2},j}$, and $(\kappa_y)_{i,j\pm\frac{1}{2}}$. Then we use the following discretization for $\nabla \cdot (|\nabla u| \nabla \kappa)$:

$$\nabla \cdot (|\nabla u| \nabla \kappa)_{i,j} \approx \frac{(g_{i+\frac{1}{2},j}(\kappa_x)_{i+\frac{1}{2},j} - g_{i-\frac{1}{2},j}(\kappa_x)_{i-\frac{1}{2},j})}{h} + \frac{(g_{i,j+\frac{1}{2}}(\kappa_x)_{i,j+\frac{1}{2}} - g_{i,j-\frac{1}{2}}(\kappa_x)_{i,j-\frac{1}{2}})}{k}.$$

Before we proceed, we need to work out a more explicit formula for V. In two dimensions, since P is the projection onto the tangent direction, we can write

$$P(x) = \langle x, \mathbf{t} \rangle \, \mathbf{t},$$

where $\mathbf{t} = \frac{(-u_y, u_x)}{|\nabla u|}$. Denote $r = \nabla \cdot (|\nabla u| \nabla \kappa)$, which we computed above. Now we have

$$\begin{aligned} V &= \frac{2}{|\nabla u|} P(\nabla(\nabla \cdot (|\nabla u| \nabla \kappa))) + |\nabla \kappa|^2 \mathbf{n} \\ &= \frac{2}{|\nabla u|} \langle \nabla r, \mathbf{t} \rangle \, \mathbf{t} + |\nabla \kappa|^2 \mathbf{n}. \end{aligned}$$

Denote $s = \langle \nabla r, \mathbf{t} \rangle$. Then

$$\begin{aligned} V^1 &= \frac{2s}{g}\mathbf{t}^1 + |\nabla\kappa|^2\mathbf{n}^1 \\ &= \frac{2s}{g^2}(-u_y) + \frac{|\nabla\kappa|^2 u_x}{g}, \end{aligned}$$

$$\begin{aligned} V^2 &= \frac{2s}{g}\mathbf{t}^2 + |\nabla\kappa|^2\mathbf{n}^2 \\ &= \frac{2s}{g^2}(u_x) + \frac{|\nabla\kappa|^2 u_y}{g}. \end{aligned}$$

Finally we compute $\nabla \cdot V$ using half-point discretizations again. Namely,

$$\nabla \cdot V_{i,j} \approx \frac{V^1_{i+\frac{1}{2},j} - V^1_{i-\frac{1}{2},j}}{h} + \frac{V^2_{i,j+\frac{1}{2}} - V^1_{i,j-\frac{1}{2}}}{k}.$$

The half-points of g and $|\nabla\kappa|^2$ are done by averaging as in the above approximation of $g_{i\pm\frac{1}{2},j}$ and $g_{i,j\pm\frac{1}{2}}$. Then we have to approximate half-points of u_x, u_y and s.

Again, let v be some function. Suppose we want to approximate $(v_x)_{i+\frac{1}{2},j}$. Then we can use

$$(v_x)_{i+\frac{1}{2},j} \approx \frac{v_{i+1,j} - v_{i,j}}{h}.$$

Similarly we can approximate $(v_x)_{i-\frac{1}{2},j}$. For $(v_x)_{i,j+\frac{1}{2}}$, we shall use

$$(v_x)_{i,j+\frac{1}{2}} \approx \text{average}(\frac{v_{i+1,j+1} - v_{i-1,j+1}}{2h}, \frac{v_{i+1,j} - v_{i-1,j}}{2h}).$$

On the other hand, it was suggested in [4] that using the following minmod approximation preserves edges better:

$$(v_x)_{i,j+\frac{1}{2}} \approx \text{minmod}(\frac{v_{i+1,j+1} - v_{i-1,j+1}}{2h}, \frac{v_{i+1,j} - v_{i-1,j}}{2h}).$$

Now we return to the half-point values of u_x, u_y and s. The half-points values of u_x, u_y can be approximated using the method mentioned above. Note that

$$s = \langle \nabla r, \mathbf{t} \rangle = r_x(-u_y) + r_y u_x,$$

which are combinations of derivatives. The half-point values of each derivative is then approximated the same way as outlined above. This finishes the discretization of $\nabla \cdot V$.

3.4 Numerical Results in images

For the disk problem in Figure 2.1, unlike the total variation solution in Figure 3.1, our proposed algorithm is able to produce a curved result.

(a) Disk Inpainting Problem (b) MCVF Solution

Figure 3.1: The disk problem and the MCVF solution

This is because the boundary of the disk (a circle) has non-zero curvature, whereas a straight line always has curvature 0. To connect with minimal change in curvature in isophotes, a non-zero curvature connection is preferred.

On the other hand, if we work with straight isophotes as in total variation inpainting, our inpainting algorithm will give a straight connection.

(a) Edge Inpainting Problem (b) MCVF Solution

Figure 3.2: Straight edge inpainting problem and the MCVF solution

Our algorithm does a very good job in restoring general images. Figure 3.3 shows an image with four bars removed, and its restoration with the MCVF. The resulting image

is natural, and curves are well-recovered (for example, the right shoulder of the person). Edges are preserved well, without much diffusion.

(a) Image

(b) MCVF Restoration

Figure 3.3: Image with four bars removed and the MCVF restoration

Next we try a more irregular inpainting domain shown in Figure 3.4. The scratches are not rectangular, and have variable widths. The MCVF recovers the picture well. However, this model again suffers from the relative size problem as in TV inpainting. When the inpainting region is too large, problems may arise. See Figure 3.5, which comes from the middle part of the rightmost scratch.

(a) Image

(b) MCVF Restoration

Figure 3.4: Image with irregular scratches and the MCVF restoration

Figure 3.5: Unnatural connection between two vegetables

As a classic example, in Figure 3.6 we show the results of the MCVF in text removal. The algorithm recovers the picture well. Sharp edges are well preserved, and the sensitivity to the change of "environment" is good.

(a) Image (b) MCVF Restoration

Figure 3.6: Image with text and the MCVF restoration

Despite the capability of the model to restore general images, the following example shows that the MCVF does not connect broken edges as well as the CDD (see Figure 3.7). The "relative size" problem reappears, although we can see that if the inpainting domain is not too large, the reconstruction of a curved arc is good (see Figure 3.8).

(a) Arc Inpainting Problem (b) MCVF Solution

Figure 3.7: Arc(thin) inpainting problem and the MCVF solution

(a) Arc Inpainting Problem (b) MCVF Solution

Figure 3.8: Arc(thick) inpainting problem and the MCVF solution

3.5 Applications to noise removal

As a bonus application, with a little modification the MCVF can be applied in image denoising. Although this is not our main focus, the result is satisfactory.

Using the same idea of total variation denoising, we add a distance term to the functional. Suppose that

$$u^0 : I \to [0, 1]$$

is some noisy image. We consider minimizing the functional

$$\Phi(u) = \int\int |\kappa|^2 |\nabla u| dxdy + \frac{\lambda}{2} \int\int |u - u^0|^2 dxdy.$$

Namely, we want to find the closest image to u^0 in L^2 that minimizes the curvature variation at the same time. Using the same argument as in Theorem 3.2.1, we can show

that the steepest descent equation is

$$\frac{\partial u}{\partial t} = \nabla \cdot V + \lambda(u^0 - u),$$

where

$$V = \frac{2}{|\nabla u|} P(\nabla(\nabla \cdot (|\nabla u| \nabla \kappa))) + |\nabla \kappa|^2 \mathbf{n},$$

$$P(x) = x - \langle x, \mathbf{n} \rangle \, \mathbf{n},$$

$$\mathbf{n} = \frac{\nabla u}{|\nabla u|}.$$

In the experiments, we used the same discretizations as described above.

In Figure 3.9(b), we have added 10 % salt and pepper noise to the image in Figure 3.9(a). The MCVF restoration, shown in 3.9(c), recovers the image very well. Edges, curved or straight, are preserved well with little or no diffusion.

In Figure 3.10 and Figure 3.11, more noise has been added to Figure 3.10(a) and 3.11(a). The image in Figure 3.10 was polluted with 30% salt and pepper noise, while that in Figure 3.11 was polluted with 40%. It is clear that the MCVF is able to identify and preserve the robust information from these amounts of noise.

(a) Original image (b) Noisy image (c) MCVF Restoration

Figure 3.9: "Lena" with 10% noise and the MCVF restoration

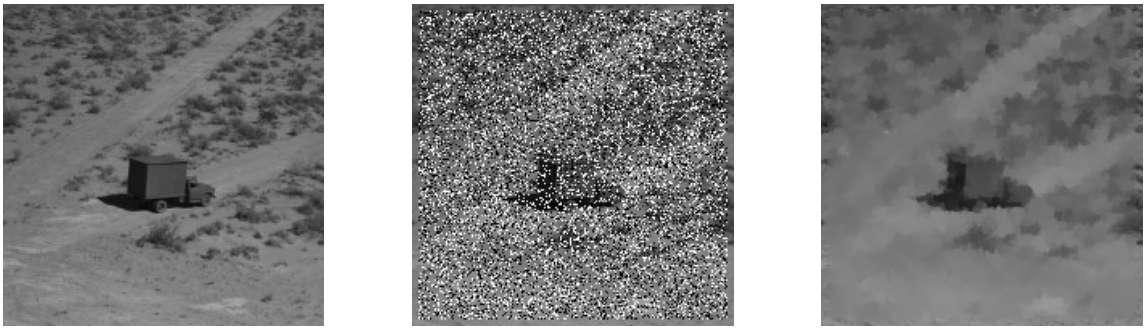

(a) Original image (b) Noisy image (c) MCVF Restoration

Figure 3.10: Image with 30% noise and the MCVF restoration

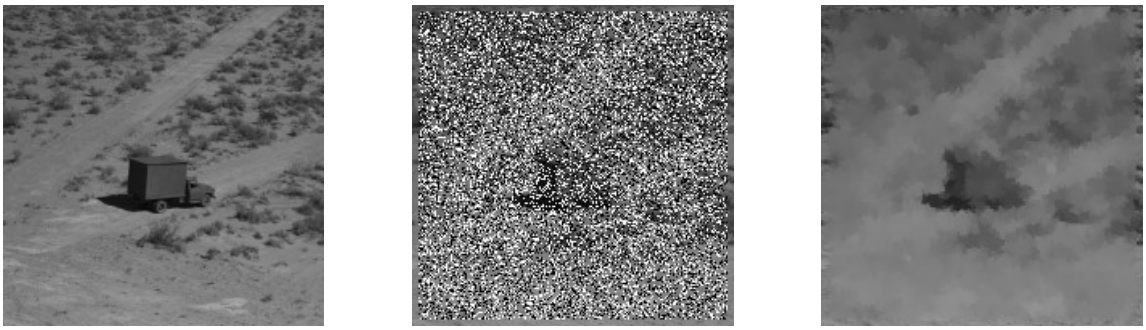

(a) Original image (b) Noisy image (c) MCVF Restoration

Figure 3.11: Image with 40% noise and the MCVF restoration

Another approach, that works for salt and pepper noise only, is as follows. Since salt and pepper noise is a random distribution of black and white pixels added to the image, we can consider the totality of these pixels as an inpainting domain. This interpretation allows us to run the MCVF on only these pixels (without the λ-term), i.e. we can consider it the same way as an inpainting problem with irregular scratches, as in Figure 3.4. These pixels can be determined by thresholding.

Figure 3.12 shows that the new approach, which can only be applied to salt and pepper noise, works extremely well in this case. The Lena example is repeated, with 30% noise. Notice how the details on her hair are preserved.

We apply this approach to the examples in Figures 3.13 and 3.14; 50% and 70% noise, respectively, are added (i.e. resp. only half and 30% information is true). The denoising results are good, and the main details are very well reconstructed.

(a) Original image (b) Noisy image (c) MCVF Restoration

Figure 3.12: "Lena" with 30% noise and the MCVF restoration

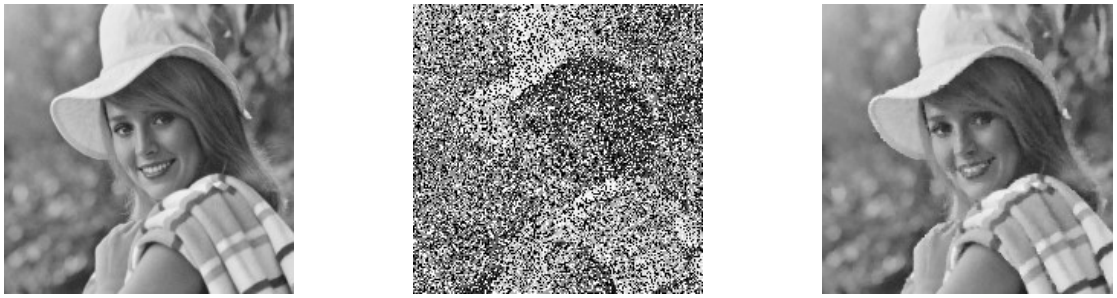

(a) Original image (b) Noisy image (c) MCVF Restoration

Figure 3.13: "Elaine" with 50% noise and the MCVF restoration

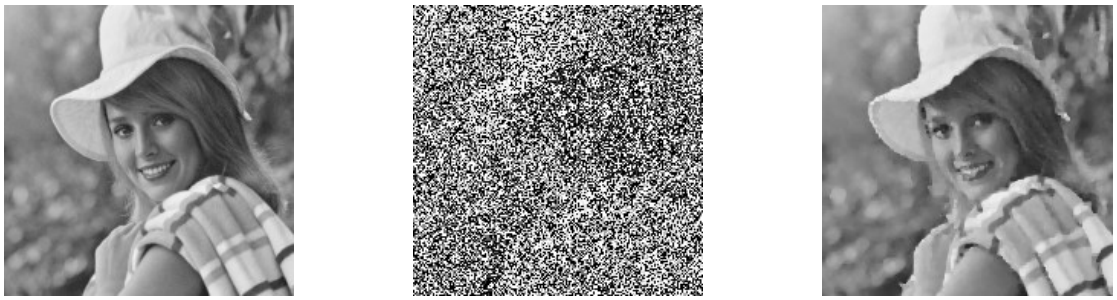

(a) Original image (b) Noisy image (c) MCVF Restoration

Figure 3.14: "Elaine" with 70% noise and the MCVF restoration

3.6 Numerical Results in 3D

In three dimensions, unlike the total variation inpainting, the MCVF is able to restore the cylinder without curving inwards. This is because the cylinder has a non-zero (mean) curvature equal to $1/r$, where r is the radius of the base circle. The total variation inpainting, while aiming to achieve the smallest intensity variation possible, ignores the curvature. The result is as in Figure 2.4.

It was also studied in Section 2.6 that a direct generalization of the Euler's elastica inpainting method also gives a distorted cylinder in the cylinder problem (see Figure 2.8). This is because both total variation inpainting and the elastica inpainting try to minimize (through the b-term) the mean curvature of the level sets.

However, since the MCVF considers the change in (mean) curvature along isophotes, the shrinking is not preferred because this model favours little variation in the curvature. Thus, in terms of restoring a cylinder, the MCVF is a better choice (see Figure 3.15). Note we were restoring a *solid* cylinder, although only the boundary of our inpainting result is shown.

In Figure 3.16, our given image is a *solid* torus (doughnut) with a section removed (the boundary is shown in the pictures). The MCVF solution is shown in Figure 3.17. This example demonstrates two properties of the MCVF:
1. "Curved" boundary surface is successfully restored.
2. Provided the gap size is not too large, the MCVF is able to connect solid objects, with disconnected parts matched correctly.

When the gap size is large, this model, as in most PDE inpainting methods, fails to connect the disconnected parts.

Finally we present a slightly different formulation of the 3D inpainting problem. We start with an initial image and a final image in an image sequence, and use the inpainting technique to fill out the middle slices. This is presented in Figure 3.18.

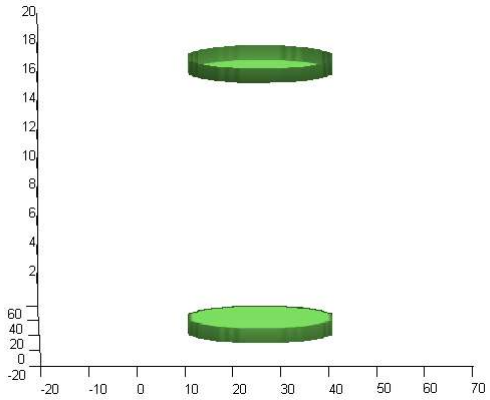

(a) Middle part to be filled in

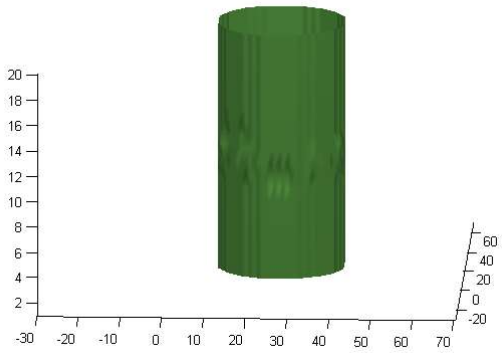

(b) MCVF Solution

Figure 3.15: Cylinder Problem and the MCVF Solution

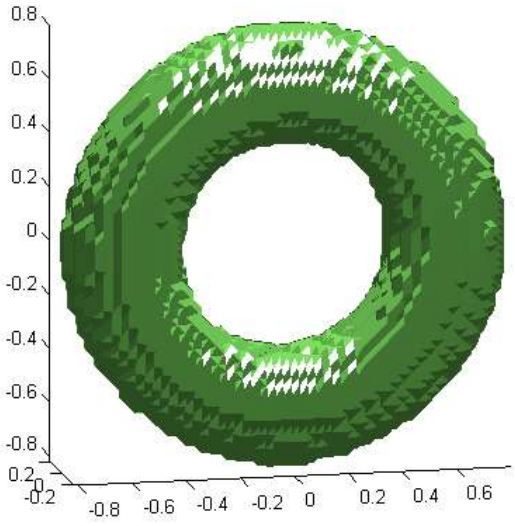

(a) Original torus

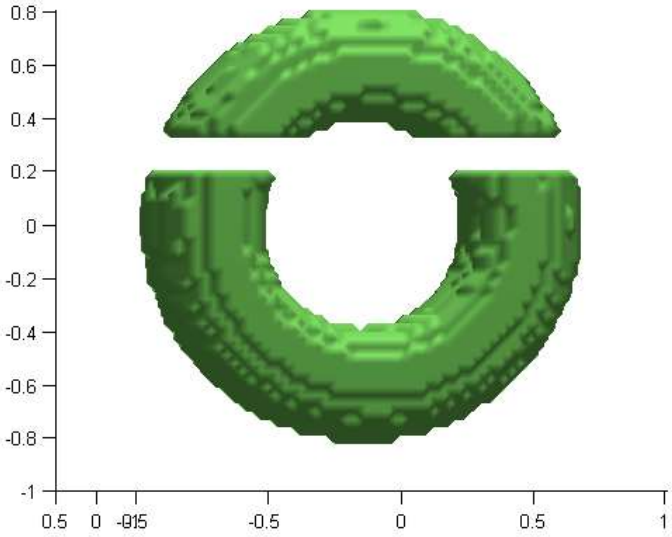

(b) Missing part to be filled in

Figure 3.16: Torus, and torus with a part removed

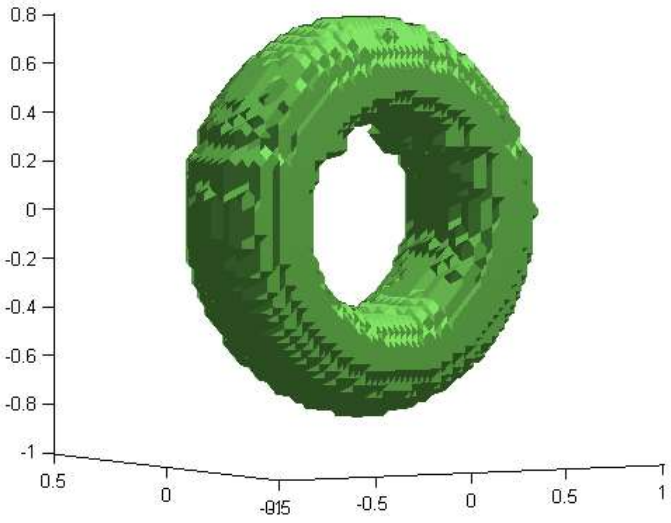

(a) MCVF Restoration, angle 1

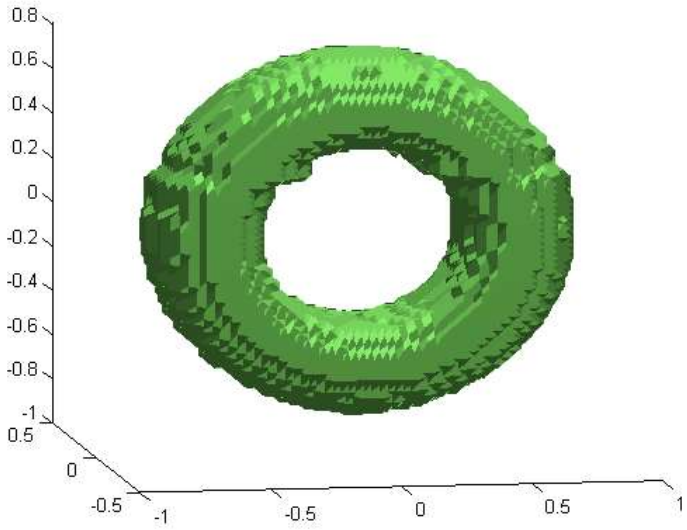

(b) MCVF Restoration, angle 2

Figure 3.17: MCVF filling of the missing part in Figure 3.16

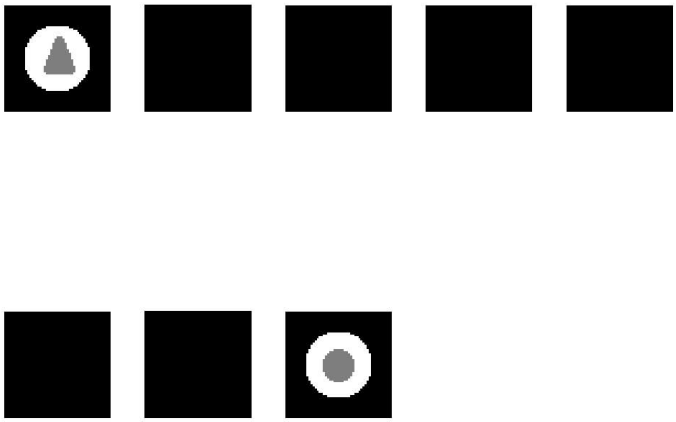

(a) Initial image sequence

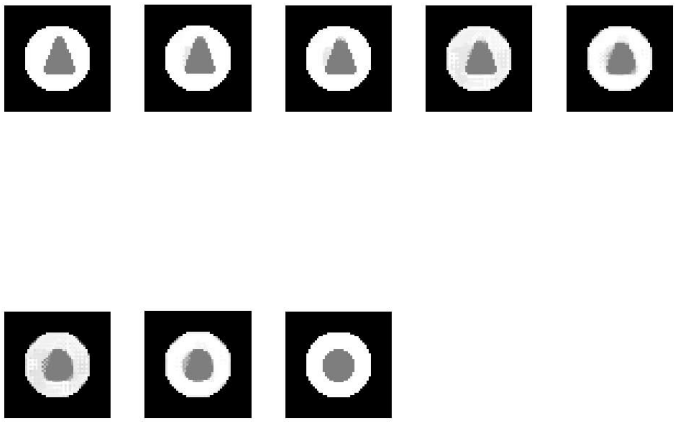

(b) Final image sequence evolved by MCVF

Figure 3.18: MCVF applied to an image sequence

Chapter 4

Summary

In the previous chapters we have reviewed the general ideas in variational inpainting methods. In particular, the total variation inpainting model and the Euler's elastica model have been studied in detail. These two models behave differently, which is a result of the different prior assumptions of the isophotes (the TV inpainting tries to complete the isophotes by straight lines, while the Euler's elastica method tries to do so through elasticas). The 3D generalizations of these methods have been studied, and we have found that these methods fail to recover a solid cylinder, which is one of the simplest, yet most important, examples in 3D inpainting.

We have then proposed a new model (MCVF), which seeks to minimize the change of curvature along isophotes. As shown in the numerical results, our new model does not only do well in general image inpainting, but also in three dimensions. The MCVF is able to recover a cylinder well, and produces nice results in other 3D inpainting problems, as shown in the examples in Section 3.6.

While the MCVF works well in these situations, we have found that the relative size problem, which is commonly found in PDE inpainting methods, remains in our new model. Information fails to propagate far across a big gap, as illustrated in Figure 3.7. In addition, due to the presence of high order spatial derivatives in the steepest descent equation, the size of time steps $\triangle t$ must be very small in order to guarantee numerical stability. For large images, the time marching is slow.

Further research includes improving the connectivity of the model (i.e. to lessen the effect of the relative size) and developing a fast implementation of the algorithm.

References

[1] Marcelo Bertalmio and Guillermo Sapiro. Image inpainting. In *Computer Graphics (SIGGRAPH 2000)*, pages 417–424, 2000.

[2] P.A. Blaga. *Lectures on the Differential Geometry of Curves and Surfaces*. Napoca Pressr, Cluj-Napoca, Romania, 2005.

[3] Folkmar Bornemann and Tom März. Fast image inpainting based on coherence transport. *J. Math. Imaging Vis.*, 28(3):259–278, July 2007.

[4] Tony F. Chan, Sung Ha Kang, and Jianhong Shen. Euler's elastica and curvature-based inpainting. *SIAM J. Appl. Math.*, 63(2):564–592 (electronic), 2002.

[5] Tony F. Chan and Jianhong Shen. Non-texture inpainting by curvature-driven diffusions (cdd). *J. Visual Comm. Image Rep*, 12:436–449, 2001.

[6] Tony F. Chan and Jianhong Shen. Mathematical models for local nontexture inpaintings. *SIAM J. Appl. Math.*, 62(3):1019–1043 (electronic), 2001/02.

[7] Tony F. Chan and Jianhong Shen. *Image processing and analysis*. Society for Industrial and Applied Mathematics (SIAM), Philadelphia, PA, 2005. Variational, PDE, wavelet, and stochastic methods.

[8] Alexei Efros, , Alexei A. Efros, and Thomas K. Leung. Texture synthesis by non-parametric sampling. In *In International Conference on Computer Vision*, pages 1033–1038, 1999.

[9] M. Elad, J.-L. Starck, P. Querre, and D. L. Donoho. Simultaneous cartoon and texture image inpainting using morphological component analysis (MCA). *Applied and Computational Harmonic Analysis*, 19:340–358, 2005.

[10] Gerhard Huisken. Flow by mean curvature of convex surfaces into spheres. *J. Differential Geom.*, 20(1):237–266, 1984.

[11] J. Jost. *Riemannian Geometry and Geometric Analysis*. Springer, United States, fifth edition, 2008.

[12] Antonio Marquina and Stanley Osher. Explicit algorithms for a new time dependent model based on level set motion for nonlinear deblurring and noise removal. *SIAM J. Sci. Comput.*, 22(2):387–405 (electronic), 2000.

[13] Leonid I. Rudin and Stanley Osher. Total variation based image restoration with free local constraints. *Proc. 1st IEEE ICIP.*, 1:31–35, 1994.

[14] Leonid I. Rudin, Stanley Osher, and Emad Fatemi. Nonlinear total variation based noise removal algorithms. *Phys. D*, 60(1-4):259–268, November 1992.

[15] V. V. Voronin, V. I. Marchuk, A. I. Sherstobitov, and K. O. Egiazarian. Image inpainting using cubic spline-based edge reconstruction. In *Proceedings of the SPIE*, volume 8295, 2012.

[16] Guoliang Xu and Qin Zhang. Minimal mean-curvature-variation surfaces and their applications in surface modeling. *GMP 2006, Lecture Notes in Computer Sciences*, 4077:357–370, 2006.